Photoluminescence of Tetrahedral Quantum-Dot Quantum Wells

Vladimir A. Fonoberov,[1,2] Evghenii P. Pokatilov,[1] Vladimir M. Fomin,[3,1,*] and Jozef T. Devreese[3,*]

[1]*Laboratory of Physics of Multilayer Structures, Department of Theoretical Physics, State University of Moldova, A. Mateevici 60, MD-2009 Chişinău, Moldova*

[2]*Nano-Device Laboratory, Department of Electrical Engineering, University of California–Riverside, Riverside, California 92521-0425, USA*

[3]*Theoretische Fysica van de Vaste Stoffen, Departement Natuurkunde, Universiteit Antwerpen, Universiteitsplein 1, B-2610 Antwerpen, Belgium*

(Received 18 June 2003; published 24 March 2004)

Taking into account the tetrahedral shape of a quantum-dot quantum well (QDQW) when describing excitonic states, phonon modes, and the exciton-phonon interaction in the structure, we obtain within a nonadiabatic approach a quantitative interpretation of the photoluminescence spectrum of a single CdS/HgS/CdS QDQW. We find that the exciton ground state in a tetrahedral QDQW is bright, in contrast to the dark ground state for a spherical QDQW. The position of the phonon peaks in the photoluminescence spectrum is attributed to interface optical phonons. We also show that the experimental value of the Huang-Rhys parameter can be obtained only within the nonadiabatic theory of phonon-assisted transitions.

DOI: 10.1103/PhysRevLett.92.127402 PACS numbers: 78.67.Bf, 63.22.+m, 73.21.La

Multilayer quantum dots (QD's) are of broad interest not only due to the striking tunability of their physical properties, but also because of the intensively investigated prospects for applications in optoelectronics, microscopy, and biology [1,2]. A quantum-dot quantum well (QDQW) has been fabricated [3] by including a layer of HgS into a nanocrystal of CdS, which has a band gap larger than that of HgS. The excitons in a QDQW are mainly confined to the HgS well, which results in a high quantum yield and an improved photochemical stability. A detailed experimental investigation of the crystalline structure, the shape, and the optical spectra can be carried out on a same single QD [4]. High-resolution transmission electron microscopy has revealed that QDQW's are preferentially tetrahedral particles [see Fig. 1(a)] with a zinc blende crystal lattice [5]. Using confocal optical microscopy, photoluminescence (PL) from a single QDQW has been measured [6]. Only the lowest excitonic transitions in spherical QDQW's have been studied theoretically [7–12] until now. In this Letter, we report the first quantitative interpretation of the PL spectrum of a QDQW.

To obtain electron and hole energy spectra in spherical QDQW's, $\mathbf{k}\cdot\mathbf{p}$ [7–9] and tight-binding [10–12] calculations have been carried out. Multiband $\mathbf{k}\cdot\mathbf{p}$ studies for spherical QDQW's yield s-type electron and p-type hole ground states [7,8], leading to the dark exciton ground state [9]. It has been shown that both multiband $\mathbf{k}\cdot\mathbf{p}$ and tight-binding calculations provide a similar qualitative physical description for the lowest states in QDQW's [12]. Recently, we used Burt's envelope-function representation to develop an eight-band theory which is particularly suitable for QD heterostructures with thin shells, consisting of materials with notably different effective-mass parameters and narrow band gaps [13]. This multiband theory was successfully applied to spherical QDQW's [8], and it is used in this Letter to study tetrahedral QDQW's.

Experiments show that the PL spectra of single QDQW's do not change appreciably for different temperatures (1.4–50 K), excitation wavelengths (442–633 nm), and intensities (0.02–50 kW/cm^2) [6]. Therefore, the spectrum corresponds to the equilibrium PL from the exciton ground state β_0. In the low-temperature limit, and using the dipole approximation, the intensities of the phonon lines in the PL spectrum of QD's are given by [14]

$$I(\Omega) \propto \sum_{K=0}^{\infty} \sum_{\lambda_1,\ldots,\lambda_K} F_{\beta_0,K}^{(\lambda_1,\ldots,\lambda_K)} \delta\Big(\Omega_{\beta_0} - \sum_{j=1}^{K} \omega_{\lambda_j} - \Omega\Big), \quad (1)$$

where K is the number of a phonon sideband and λ_j labels the phonon modes with frequencies ω_{λ_j}. The general expression for the amplitudes F of the phonon lines is given in Ref. [14]. For the zero-phonon line ($K = 0$) and for the one-phonon lines ($K = 1$), these amplitudes are given by

$$F_{\beta_0,0} = |d_{\beta_0}|^2, \quad (2)$$

$$F_{\beta_0,1}^{(\lambda_1)} = \sum_{\beta_1,\beta_2} \frac{\hbar^{-2} d_{\beta_1}^* d_{\beta_2} \langle\beta_1|\gamma_{\lambda_1}|\beta_0\rangle\langle\beta_0|\gamma_{\lambda_1}^*|\beta_2\rangle}{(\Omega_{\beta_0} - \Omega_{\beta_1} - \omega_{\lambda_1})(\Omega_{\beta_0} - \Omega_{\beta_2} - \omega_{\lambda_1})}, \quad (3)$$

where γ_{λ_j} are the amplitudes of the exciton-phonon interaction. The dipole matrix element d_β is given by

$$d_\beta \propto \int \delta(\mathbf{r}_e - \mathbf{r}_h)(\mathbf{e}, \hat{\mathbf{p}})\Psi_{\text{exc}}^{(\beta)}(\mathbf{r}_e, \mathbf{r}_h) d\mathbf{r}_e d\mathbf{r}_h, \quad (4)$$

where $\mathbf{e}$ denotes the light polarization vector and $\hat{\mathbf{p}}$ is the

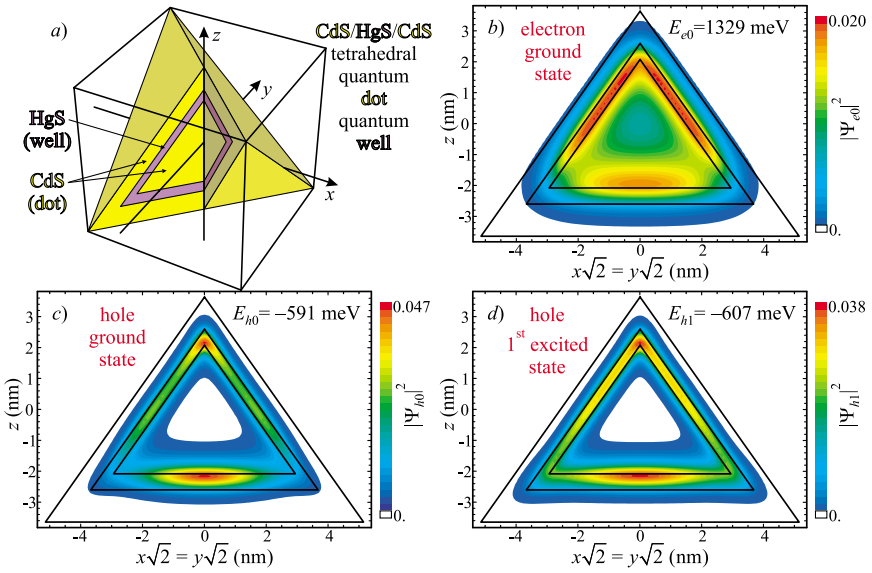

FIG. 1 (color). The tetrahedral quantum-dot quantum well (a) and the average probability densities in the plane $x = y$ of an electron on the twofold degenerate ground state level E_{e0} (b), and a hole on the fourfold degenerate ground state and first excited state levels E_{h0} (c), and E_{h1} (d). A quarter ($y < x < -y$) of the tetrahedron in (a) is removed to show the position of the HgS shell. The factor of $\sqrt{2}$ multiplying the x and y coordinates in (b)–(d) is used to keep the same scale with the z coordinate.

momentum operator [15]. $\Psi_{\rm exc}^{(\beta)}$ is the wave function for an exciton state β with energy $\hbar\Omega_\beta$; it is a sum of products of envelope and Bloch functions. For symmetric QD's (e.g. spherical or tetrahedral) the dependence of the dipole matrix element (4) on $\mathbf{e}$ reduces to a constant multiplier, which does not affect the relative intensities of the PL peaks.

It is convenient to choose the origin of the coordinate system in the center of the QDQW [see Fig. 1(a)], and to introduce the coordinate $\xi = (\mathbf{n}_f, \mathbf{r})$, where $\mathbf{n}_f$ is the outward unit vector of the normal to a tetrahedron's facet that contains the point with radius vector $\mathbf{r}$. The isosurface of constant ξ is a tetrahedron circumscribed around a sphere with radius ξ. In this Letter we consider a CdS/HgS/CdS QDQW with the dimensions determined in Refs. [5,6], namely, a CdS core, a HgS shell, and an outer CdS shell bounded by tetrahedrons with $\xi_1 = 1.2$ nm, $\xi_2 = 1.5$ nm, and $\xi_3 = 2.1$ nm. The thicknesses of the HgS shell and of the outer CdS shells are $\xi_2 - \xi_1 = 0.3$ nm (1 monolayer) and $\xi_3 - \xi_2 = 0.6$ nm (2 monolayers).

The exciton energies and wave functions have been derived numerically from the Hamiltonian:

$$\hat{H}_{\rm exc} = [\hat{H}_e + V_{\rm s-a}(\mathbf{r}_e)] - [\hat{H}_h - V_{\rm s-a}(\mathbf{r}_h)] + V_{\rm int}(\mathbf{r}_e, \mathbf{r}_h), \tag{5}$$

where $\hat{H}_e$ is the two-band electron Hamiltonian and $\hat{H}_h$ is the six-band hole Hamiltonian, which we derived from a general eight-band Hamiltonian for heterostructures [13]. The dielectric mismatch between QDQW shells leads to the electron and hole self-interaction potential $V_{\rm s-a}$ and significantly changes the potential of the electron-hole interaction $V_{\rm int}$ [16]. The effective-mass parameters for CdS are taken from Ref. [16], the dielectric constants from Ref. [17], and all other required parameters from Ref. [8]. The effective-mass parameters for HgS entering the Hamiltonians $\hat{H}_e$ and $\hat{H}_h$ are calculated as a function of the energies of the electron and the hole ground states. The numerical calculation is carried out using a finite-difference method on the same cubic mesh, both inside and outside the QDQW, as for tetrahedral CdS QD's [16]. A mesh length of $0.05\sqrt{3}$ nm ensures a relative error for the exciton ground state energy less than 1%.

HgS is a quantum well for both electrons and holes in the QDQW. While only a few electron states lie below the CdS bulk conduction band edge and are localized near the HgS shell, many hole states are trapped in the HgS shell and lie above the CdS bulk valence band edge. It is seen from Figs. 1(b) and 1(c) that the electron in the ground state is practically uniformly distributed in the HgS shell while the hole in the ground state is localized near the edges of the tetrahedral HgS shell. Figure 1(d) shows that, unlike in the ground state, the hole in the first

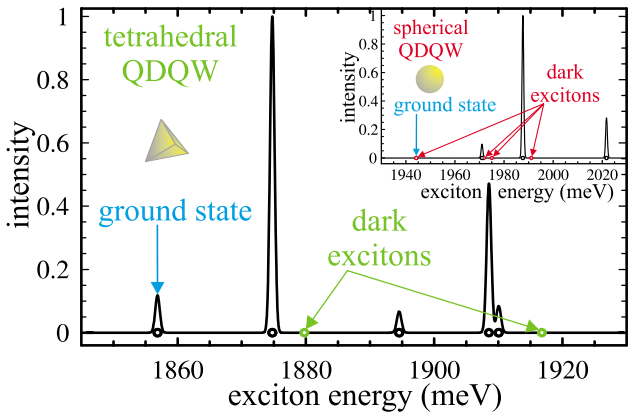

FIG. 2 (color). Normalized intensities of the lowest exciton levels in the optical absorption spectrum of a tetrahedral QDQW (the inset gives the intensities for the spherical QDQW considered in Ref. [8]). Spectral lines are broadened by a Gaussian to enhance visualization.

excited state substantially penetrates the region of facets of the HgS shell, where the electron density in the ground state is high.

In the QDQW's optical absorption spectrum, the intensity of a transition to the exciton level β is $|d_\beta|^2$. Figure 2 shows that the intensity of the second exciton level is ~8.5 times larger than that of the ground state level. Since the second exciton state is absorbing and the exciton ground state is luminescing, a Stokes shift should be observed between the frequencies of the excitation and the zero-phonon equilibrium PL. In addition to the fact that our calculated exciton ground state energy of 1857 meV is in excellent agreement with the experimental data of Refs. [5,6], the obtained excitation energy of 18 meV is very close to the value 19 meV of the Stokes shift found in the fluorescence line narrowing spectrum [5]. The inset of Fig. 2 shows the result of an analogous finite-difference calculation of the exciton states for a spherical QDQW [8] with the same thickness of the HgS shell as that for the tetrahedral QDQW. The exciton ground state is eightfold degenerate for both spherical and tetrahedral QDQW's. The remarkable effect of the QDQW's shape is that the exciton in the ground state is bright for the tetrahedral QDQW, while it is dark for the spherical QDQW. We find that the ratio of the intensity of the exciton ground state to the intensity of the first excited state is very sensitive to the shape of the QDQW's. This sensitivity determines the crucial role of the shape of QDQW's also for their PL spectra.

The amplitudes of the exciton-phonon interaction are $\gamma_\lambda(\mathbf{r}_e, \mathbf{r}_h) \equiv V_\lambda(\mathbf{r}_e) - V_\lambda(\mathbf{r}_h)$. In the dielectric continuum approach, the amplitudes $V_\lambda(\mathbf{r}_e)$ of the electron-phonon interaction, $V_\lambda(\mathbf{r}_h)$ of the hole-phonon interaction, and the phonon frequency ω_λ are solutions of the eigenvalue problem for the equation

$$\nabla(\varepsilon(\omega_\lambda)\nabla V_\lambda) = 0 \quad \text{with } \varepsilon(\omega) = \varepsilon_\infty \frac{\omega^2 - \omega_{\mathrm{LO}}^2}{\omega^2 - \omega_{\mathrm{TO}}^2}, \qquad (6)$$

where, for each shell, ω_{LO} and $\omega_{\mathrm{TO}} \equiv \omega_{\mathrm{LO}}\sqrt{\varepsilon_\infty/\varepsilon_0}$ are the frequencies of the bulk longitudinal optical (LO) and the transverse optical (TO) phonons, and ε_0 and ε_∞ are the static and the high-frequency dielectric constants, respectively. There exist two kinds of solutions of Eq. (6). Solutions of the first kind $[\varepsilon(\omega_\lambda) = 0]$ describe bulklike phonon modes [18]. In the kth shell they have the frequency $\omega_{\mathrm{LO}}^{(k)}$ and their amplitude is chosen to satisfy the equation $\nabla^2 V_\lambda = -q_k^2 V_\lambda$ with boundary conditions $V_\lambda|_{\xi\notin[\xi_{k-1},\xi_k]} = 0$. The number of bulklike phonon modes is restricted by the condition $q_k \le \pi/a$, where a is the lattice constant. Solutions of the second kind $[\varepsilon(\omega_\lambda) \neq 0]$ describe interface phonon modes. To the best of our knowledge, the phonons for the tetrahedral QDQW are theoretically derived here for the first time. We propose for the tetrahedral QDQW an approximation with a spatial behavior close to that for spherical QD's, i.e., s-like, p-like, etc. This means that we seek interface phonon modes as a product of a function $\Phi(\xi)$, which is constant on the tetrahedral surface $S(\xi)$, and a function $\varphi(\mathbf{r})$, which satisfies the equation $\nabla^2\varphi_Q = -q^2\varphi_Q$ and which is zero at infinity. If this method is applied to a spherical QDQW, where $\xi \equiv r$, $\Phi(\xi)$ turns out to be a radial function and $\varphi(\mathbf{r})$ explicitly contains the spherical harmonics that define the spatial symmetry. Substituting $V_\lambda = \Phi(\xi)\,\varphi_Q(\mathbf{r})$ into Eq. (6), multiplying by φ_Q^* and integrating over the tetrahedral surface $S(\xi)$, we obtain a one-dimensional problem with eigenfrequencies $\omega_{Q,n}$ and eigenfunctions $\Phi_{Q,n}(\xi)$. We used the frequencies of the LO phonons found in Ref. [5]. For the numerical calculation of the bulklike and interface phonon modes we have used the same finite-difference scheme as described above. For any spatial symmetry of φ_Q we found five different functions $\Phi_{Q,n}$ that correspond to five eigenfrequencies $\omega_{Q,n}$ $(n = 1, \ldots, 5)$ of the interface phonons. Figure 3 shows the amplitudes of the interface phonon modes $V_{Q,n}$ with p-like spatial symmetry, averaged over the tetrahedral surface $S(\xi)$. In contrast to the amplitudes of the bulklike phonon modes that vanish at the boundaries, the amplitudes of the interface phonon modes have their extremal values at some of the boundaries.

In Fig. 4 the PL spectrum calculated using Eq. (1) for a single tetrahedral QDQW is compared with two experimental spectra, measured at different excitation wavelengths and intensities [6,19]. Most likely spectral diffusion, which has been explained recently by a reorganization of local electric fields in or around the particles [20], is responsible for the relatively broad lines in the PL spectra of a single QDQW. The experimentally determined Huang-Rhys parameter is 0.25 ± 0.05 [6]. Because of the localization of the exciton in the HgS well, the amplitudes of the bulklike phonon modes are much smaller than those of the interface phonon modes. The dominant contribution to the intensity of the

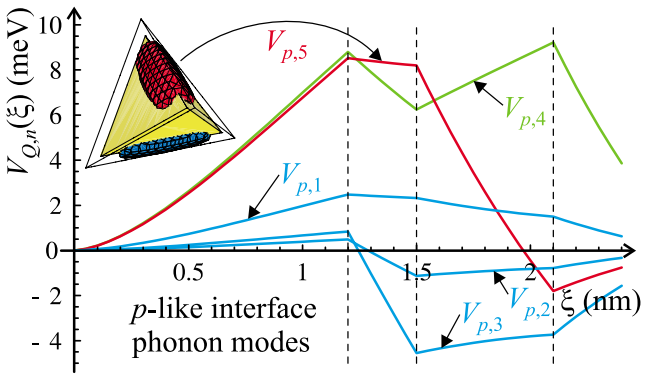

FIG. 3 (color). Amplitudes of several interface phonon modes averaged as $V_{Q,n}(\xi) = \Phi_{Q,n}(\xi)\sqrt{\int_{S(\xi)} |\varphi_Q|^2 dS / \int_{S(\xi)} dS}$ (for denotations see text). Vertical dashed lines show the boundaries of the tetrahedral shells. Isosurfaces $V_{p_z,5}(\mathbf{r}) = 10$ meV (red) and $V_{p_z,5}(\mathbf{r}) = -10$ meV (blue) in the HgS shell are shown. The amplitudes $V_{p,4}$ and $V_{p,5}$ give the highest one-phonon peaks in the PL spectrum in Fig. 4.

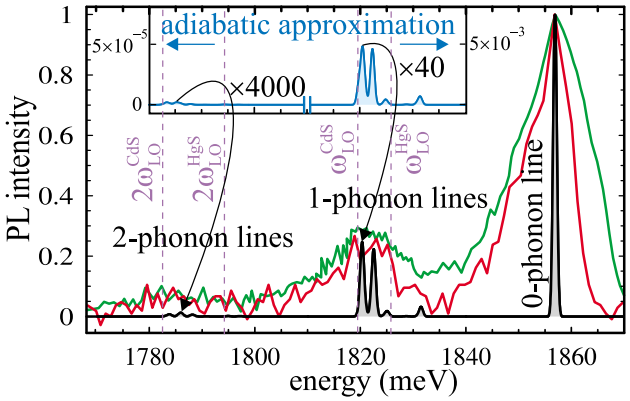

FIG. 4 (color). PL spectrum of a tetrahedral QDQW normalized to the zero-phonon line's intensity. Calculated spectral lines (black curve) are broadened by a Gaussian to facilitate visualization. Experimental spectra are measured at $T = 10$ K with excitation wavelength 633 nm and intensity 15 kW/cm^2 (green curve) [6] and with excitation wavelength 442 nm and intensity 5 kW/cm^2 (red curve) [19]. The inset gives one- and two-phonon bands (magnified by factors of 40 and 4000, respectively) as calculated within the adiabatic approximation.

one-phonon lines in the calculated PL spectrum is due to p-like interface phonon modes. The two most intense one-phonon peaks correspond to the modes with amplitudes $V_{p,4}$ and $V_{p,5}$ in Fig. 3 and energies 34.3 and 36.7 meV, respectively. The average energy, weighted with the intensities of the two peaks, is 35.5 meV, in good agreement with the experimentally determined value of 35.3 ± 0.6 meV [6]. The intensity of the calculated two-phonon lines cannot directly be compared with that in the experimental spectra because of the large background in this spectral region. The inset of Fig. 4 shows the one- and two-phonon bands in the PL spectrum calculated within the *adiabatic approximation*. In this approximation, the intensities of the one-phonon peaks are defined by Eq. (3), however, without the summation over the states β_1 and β_2, which are replaced by β_0. Since the exciton ground state β_0 is eightfold degenerate and its intensity $|d_{\beta_0}|^2$ is small as compared to the intensities of the higher lying exciton states (see Fig. 2), the intensities of the phonon peaks in the adiabatic approximation are dramatically lower than those calculated within the nonadiabatic theory [14].

In summary, we have shown a strong difference between the optical spectra of spherical and tetrahedral QDQW's. Only the simultaneous consideration of the tetrahedral shape of a QDQW, interface optical phonons, and nonadiabatic phonon-assisted transitions allows for profound understanding of the optical response of a QDQW. In particular, this analysis allowed us to interpret the observed PL spectra of a CdS/HgS/CdS QDQW.

The authors thank T. Basché for fruitful communications and for the provided experimental data. Discussions with F. Brosens, V. N. Gladilin, S. N. Klimin, J. H. Wolter, and A. A. Balandin are gratefully acknowledged. E. P. P. and V. A. F. acknowledge with gratitude the kind hospitality received during their visit to the Universiteit Antwerpen (UIA). This work has been supported by the GOA BOF UA 2000, IUAP, FWO-V Projects No. G.0274.01, No. G.0435.03, the W.O.G. WO.025.99N (Belgium), the EC GROWTH Programme, NANOMAT Project No. G5RD-CT-2001-00545, and the MRDA-CRDF Grant No. MP2-3044 (Moldova).

*Also at COBRA, TU Eindhoven, P.O. Box 513, 5600 MB Eindhoven, The Netherlands.

[1] A. P. Alivisatos, Science **271**, 933 (1996).
[2] M. Bruchez, M. Moronne, P. Gin, S. Weiss, and A. P. Alivisatos, Science **281**, 2013 (1998).
[3] A. Eychmüller, A. Mews, and H. Weller, Chem. Phys. Lett. **208**, 59 (1993).
[4] F. Koberling, A. Mews, G. Philipp, U. Kolb, I. Potapova, M. Burghard, and T. Basché, Appl. Phys. Lett. **81**, 1116 (2002).
[5] A. Mews, A. V. Kadavanich, U. Banin, and A. P. Alivisatos, Phys. Rev. B **53**, R13 242 (1996).
[6] F. Koberling, A. Mews, and T. Basché, Phys. Rev. B **60**, 1921 (1999).
[7] W. Jaskolski and G.W. Bryant, Phys. Rev. B **57**, R4237 (1998).
[8] E. P. Pokatilov, V. A. Fonoberov, V. M. Fomin, and J. T. Devreese, Phys. Rev. B **64**, 245329 (2001).
[9] J. T. Devreese, V. M. Fomin, V. N. Gladilin, E. P. Pokatilov, and S. N. Klimin, Nanotechnology **13**, 163 (2002).
[10] J. Pérez-Conde and A. K. Bhattacharjee, Phys. Status Solidi B **229**, 485 (2002).
[11] R. H. Xie, G.W. Bryant, S. Lee, and W. Jaskolski, Phys. Rev. B **65**, 235306 (2002).
[12] G.W. Bryant and W. Jaskólski, Phys. Rev. B **67**, 205320 (2003).
[13] E. P. Pokatilov, V. A. Fonoberov, V. M. Fomin, and J. T. Devreese, Phys. Rev. B **64**, 245328 (2001).
[14] V. M. Fomin, V. N. Gladilin, J. T. Devreese, E. P. Pokatilov, S. N. Balaban, and S. N. Klimin, Phys. Rev. B **57**, 2415 (1998).
[15] Al. L. Efros, M. Rosen, M. Kuno, M. Nirmal, D. J. Norris, and M. Bawendi, Phys. Rev. B **54**, 4843 (1996).
[16] V. A. Fonoberov, E. P. Pokatilov, and A. A. Balandin, Phys. Rev. B **66**, 085310 (2002).
[17] L. Zhang, H. J. Xie, and C. Y. Chen, Phys. Rev. B **66**, 205326 (2002).
[18] S. N. Klimin, E. P. Pokatilov, and V. M. Fomin, Phys. Status Solidi B **184**, 373 (1994).
[19] T. Basché (private communications).
[20] R. G. Neuhauser, K. T. Shimizu, W. K. Woo, S. A. Empedocles, and M. G. Bawendi, Phys. Rev. Lett. **85**, 3301 (2000).